JOURNAL OF BIOMOLECULAR STRUCTURE AND DYNAMICS
https://doi.org/10.1080/07391102.2020.1845976

Taylor & Francis
Taylor & Francis Group

Reprofiling of approved drugs against SARS-CoV-2 main protease: an in-silico study

Prateek Kumar[a], Taniya Bhardwaj[a], Ankur Kumar[a], Bhuvaneshwari R. Gehi[a], Shivani K. Kapuganti[a], Neha Garg[b], Gopal Nath[c] and Rajanish Giri[a]

[a]School of Basic Sciences, Indian Institute of Technology Mandi, Mandi, Himachal Pradesh, India; [b]Department of Medicinal Chemistry, Faculty of Ayurveda, Institute of Medical Sciences, Banaras Hindu University, Varanasi, India; [c]Department of Microbiology, Faculty of Medicine, Institute of Medical Sciences, Banaras Hindu University, Varanasi, India

Communicated by Ramaswamy H. Sarma

ABSTRACT

Given the COVID-19 pandemic, currently, there are many drugs in clinical trials against this virus. Among the excellent drug targets of SARS-CoV-2 are its proteases (Nsp3 and Nsp5) that plays vital role in polyprotein processing giving rise to functional nonstructural proteins, essential for viral replication and survival. Nsp5 (also known as M^{pro}) hydrolyzes replicase polyprotein (1ab) at eleven different sites. For targeting M^{pro}, we have employed drug repurposing approach to identify potential inhibitors of SARS-CoV-2 in a shorter time span. Screening of approved drugs through docking reveals Hyaluronic acid and Acarbose among the top hits which are showing strong interactions with catalytic site residues of M^{pro}. We have also performed docking of drugs Lopinavir, Ribavirin, and Azithromycin on SARS-CoV-2 M^{pro}. Further, binding of these compounds (Hyaluronic acid, Acarbose, and Lopinavir) is validated by extensive molecular dynamics simulation of 500 ns where these drugs show stable binding with M^{pro}. We believe that the high-affinity binding of these compounds will help in designing novel strategies for structure-based drug discovery against SARS-CoV-2.

Abbreviations: COVID-19: Coronavirus Disease 2019; SARS-CoV-2: Severe Acute Respiratory Syndrome Coronavirus 2; M^{pro}: Non Structural Protein 5; XP: Extra Precision; MD: Molecular Dynamics; RMSD: Root Mean Square Deviation; RMSF: Root Mean Square Fluctuation; Rg: Radius of Gyration; PCA: Principle Component Analysis; SASA: Solvent Accessible Surface Area; Dscore: Druggability Score; HA: Hyaluronic Acid

ARTICLE HISTORY
Received 15 May 2020
Accepted 30 October 2020

KEYWORDS
SARS-CoV-2; COVID-19; Nsp5; Mpro; approved drug; protease

Introduction

Traditional drug development, despite of technical advancement is an expensive, laborious, and time-consuming process. In the pandemic situation like Coronavirus Disease 2019 (COVID-19), where no proper cure is available, drug repurposing or repositioning of an approved drug is a desirable choice. Repurposing is a progressive strategy that helps in identifying a new use for already approved drugs. With undeniable advantages of shorter time requirements and lower costs for development, use of an approved drug against a novel target can fulfill the principle need in this current pandemic (Ashburn & Thor, 2004; Breckenridge & Jacob, 2019; Pushpakom et al., 2019). Therefore, drug repurposing against different targets of newly emerged Severe Acute Respiratory Syndrome Coronavirus 2 (SARS-CoV-2) may deliver faster results.

Our previous report on SARS-CoV-2 has elaborately discussed the identified or probable functions and presence of disorder in its proteome (Giri et al., 2020). Among the known protein targets of SARS-CoV-2, non structural protein 3 and 5 (also called as M^{pro} or 3CL-protease) proteases are excellent drug targets due to their roles in processing of polyprotein into the constituent nonstructural proteins needed for viral replication and survival (Wu et al., 2020). M^{pro} cleaves the replicase polyprotein 1ab at eleven different sites and is considered to be the best-characterized enzyme targets for drug development against coronaviruses (Zhang et al., 2020). Recently, one of the crystal structures of SARS-CoV-2 M^{pro} (PDB ID: 6LU7) in complex with N3 (asynthetic inhibitor) is reported by Zhenming et al. (Anand et al., 2003; Jin et al., 2020).

Previously, we have established several studies to identify some of the existing drugs as inhibitors of other viral proteomes (Kumar et al., 2018, 2019; Kumar, Sharma et al., 2020; Sharma et al., 2020). One such report discussed the inhibitory action of hydroxychloroquine against Zika virus protease (Kumar et al., 2018). Here, in this study, we made an attempt to identify druggable sites in M^{pro} and also investigated the binding interactions between M^{pro} and approved drug molecules. We have screened a library of drugs approved by USA, Canada and European authorities, fetched from the Drugbank database, against active-site of SARS-CoV-2 M^{pro}. As revealed from docking and simulation results, top hit

CONTACT Rajanish Giri rajanishgiri@iitmandi.ac.in School of Basic Sciences, Indian Institute of Technology Mandi, Mandi, Himachal Pradesh 175005, India

compounds and approved drugs (which are currently in clinical trials) (Cao et al., 2020; 'COVID-19 ring-based prevention trial with lopinavir/ritonavir', 2020; 'Evaluation of the efficacy of the hydroxychloroquine-azithromycin combination in the in the prevention of COVID-19 related SDRA', 2020; Khalili et al., 2020; 'Safety and efficacy of hydroxychloroquine associated with azithromycin in SARS-CoV2 virus', 2020) are showing stable and robust binding with active site residues of enzyme M^{pro}. High-affinity binding interactions of these compounds could be a basis to design or improve the novel strategies for further clinical trials and structure-based drug discovery against SARS-CoV-2.

Materials and methods

Preparation of protein and ligands

First crystal structure of SARS-CoV-2 main protease (PDB ID: 6LU7) (Jin et al., 2020) in complex with N3 inhibitor is made available quickly for exploring structure-based drug designing opportunities. The structure is prepared and refined using *Protein Preparation Wizard* of Schrodinger LLC (Madhavi Sastry et al., 2013). The improper bond parameters and sidechain disarrangement in M^{pro} structure are corrected in Maestro and minimized by OPLS 2005 forcefield. The M^{pro} structure is used to generate active sites from Sitemap program (Halgren, 2009). A grid is generated at the inhibitor binding site to analyze the interactions of approved drugs with the active site of M^{pro}. A library of 2454 approved drugs obtained from Drugbank database (Wishart et al., 2018) is prepared in *LigPrep* module by generating at most 4 stereoisomers and tautomers (total 5025 structure in output) per ligand at pH 7 using Epik program.

Docking studies of m^{pro} with approved drugs

Prepared library of approved drugs is docked against prepared M^{pro} structure using Glide XP (Extra Precision method) scoring algorithm embedded in Schrodinger. OPLS 2005 forcefield is used for calculating bonded and non-bonded parameters such as van der Waal interactions (Friesner et al., 2006; Halgren et al., 2004). For the detailed protocol of Glide, see our previously reported articles (Kumar et al., 2019; Kumar, Aarthy et al., 2020; Kumar, Saumya et al., 2020; Sharma et al., 2017; Yadav et al., 2020). The interaction of docked compounds with M^{pro} is analyzed in the 4 Å cutoff of active site. Further, binding energy calculation is done using Prime module (based on Molecular mechanics-Generalized Born Surface Area: MM-GBSA) (Aarthy et al., 2018; Jacobson et al., 2004).

Molecular dynamics (MD) simulations

To study the structural dynamics and binding stability of inhibitors with M^{pro} at a molecular level, we performed MD simulation in SPC water models using GROMOS54A7 forcefield in Gromacs upto 500 ns (Berendsen et al., 1995). Charge neutralization is done by adding 3 Na^+ ions and 0.15 M salt in the cubic simulation box. For energy minimization, 50,000 steps of steepest descent algorithm are executed with Verlet cutoff scheme to calculate the neighboring interactions. Further, equilibration process under NPT and NVT conditions is done for 1 ns. Parrinello-Rahman and V-rescale methods are availed for pressure and temperature coupling, respectively. The inhibitor topologies are generated using PRODRG server. Finally, the production runs for all four systems (M^{pro} with Hyaluronic acid (HA), Acarbose, Amikacin, and Lopinavir) is performed in periodic boundary conditions for 500 ns each. LINCS algorithm is used for calculating bond parameters (Hess et al., 1997). Particle Mesh Ewald for long-range electrostatics with fourier spacing of 0.16 is used for production MD simulations.

Analysis of MD simulations

The analysis consisting root mean square deviation (RMSD), root mean square fluctuation (RMSF), radius of gyration (Rg) for C-α atoms, are calculated using gmx, rms, rmsf, and gyrate commands, respectively. The number of hydrogen bonds are calculated in VMD using Hydrogen bonds plugin (Humphrey et al., 1996). Further, we have used covar and anaeig commands of gromacs to interpret the cumulative motions occurring in protein by virtue of ligand binding describing the principle component analysis (PCA). We have also measured the solvent accessible surface area (SASA) using sasa command in Gromacs to determine the exposed surface area of protein to the solvents.

Results and discussion

Analysis of active site and other druggable sites of m^{pro}

The M^{pro} crystal structure (PDB ID: 6LU7) is used in this study to screen the approved drug molecules for the purpose of identifying a potential inhibitor candidate. To proceed with the screening process, identification of a druggable site is the primary requirement for a potent outcome. As illustrated in Figure 1, five different druggable sites are predicted in M^{pro} structure by employing a SiteMap module. Among these five predicted sites, the most appropriate site based on the size and volume of the pocket, hydrophobicity and hydrophilicity of amino acid, site score, and druggability score (Dscore) is selected for docking and simulation analyses (Table 1). Out of all five sites, site 1 obtains the highest site score and Dscore. Importantly, it consists of a catalytic dyad having -His41 and -Cys145, essential for the protease activity of M^{pro}. Also, a comparison between the predicted site 1 and inhibitor binding site of N3 (co-crystallized N3 inhibitor with M^{pro}; 6LU7) reveals a similar type of residue distribution in both sites (Table 1). Therefore, we have considered site 1 for further docking studies. A grid was generated at site 1 with the coordinates of −12.49 Å, 15.06 Å and 74.04 Å for X, Y and Z, respectively.

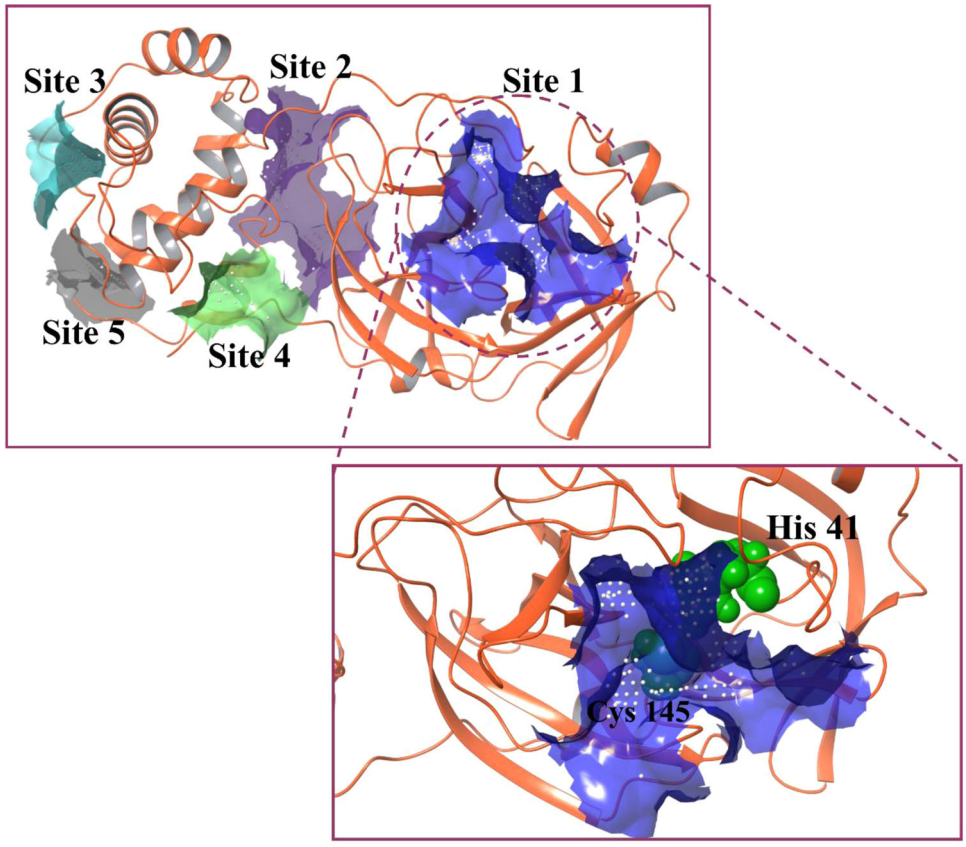

Figure 1. Predicted druggable sites of M^{pro}. Five druggable sites are represented with different colors – site 1: blue; site 2: purple; site 3: cyan; site 4: green and site 5: grey. Site 1 shows the highest site score and Dscore, and hence is selected for docking studies.

Table 1. Parameters associated with druggable site of M^{pro} predicted by SiteMap.

Druggable sites	Site score	Dscore	Hydro-phobicity	Hydro-philicity	Residue distribution at the druggable site
N3 binding site (6LU7)	–	–	–	–	3, 4, **24–27**, **41**, **49**, **140–145**, **163–166**, **172**
Site 1	0.99	1.036	0.699	0.876	**25–27**, **41**, 44–46, **49**, 52, 54, **140–145**, **163–168**, **172**, 187–190, 192
Site 2	0.782	0.769	0.279	0.875	8, 104, 106–111, 127, 151, 153, 158, 200–203, 240, 246, 249, 292–295
Site 3	0.645	0.61	0.873	0.749	218–221, 270–271, 274–277, 279
Site 4	0.573	0.385	0.09	1.352	3–5, 207, 282, 284, 288, 291
Site 5	0.541	0.444	0	1.102	212–213, 217, 256–257, 304–306

Residue distribution in predicted site 1 and experimental N3 binding site is observed to be very similar. Residues of active site in crystal structure and predicted active site, in bold fonts, show similarity with each other.

Molecular docking

2454 approved drug molecules are selected from DrugBank database for molecular docking at predicted site 1 of M^{pro} of SARS-CoV-2. These selected drugs are first subjected to the ligand preparation module, *Ligprep*, to generate at most four stereoisomers for each drug molecule (produced 5025 structures). Resulted structures are then subjected further in molecular docking protocol, which generated 9263 binding poses from 5025 input structures based on binding energies. Based on their interactions and docking scores, we have shortlisted top 100 hits which are tabulated in Table 2. Most of these listed compounds are antibiotics and antioxidants or have anti-inflammatory as well as anti-cancer properties (Table 2). In addition to top 100 compounds we have also shortlisted Ribavirin, Lopinavir, and Azithromycin (Table 3) for further analysis as these approved drugs are currently being tested on SARS-CoV-2 infected patients. The investigation of stability and binding interactions of these compounds at M^{pro} active site 1 will help in designing novel strategies for therapeutics against COVID-19. Detailed description of docking parameters of top hits and selected compounds are given in Tables 2 and 3.

Hyaluronic acid (HA): It is an anionic non-sulfated linear glycosaminoglycan polymer of two saccharide units, D-glucuronic acid and N-acetyl-d-glucosamine. HA is stabilized at the active site 1 of M^{pro} via hydrogen bonds (H-bonds) with Ser46, Thr24, Thr25, Thr26, Asn142 and Glu166 residues (Figure 2). HA shows docking score and binding energy equivalent to −13.54 kcal/mol and −49.46 kcal/mol, respectively (Table 2). It is majorly found in connective tissues, umbilical cord, vitreous fluid in eyes, and synovial fluid of joints (Fraser et al., 1997). Due to its presence in the extracellular matrix, HA is biocompatible and biodegradable, and therefore, functions as a drug delivery carrier (Widjaja et al., 2014). Using cell culture studies, HA has been demonstrated to work as an antiviral compound against both DNA and RNA viruses such as Coxsackievirus B5, Herpes Simplex Virus

Table 2. A summary of XP-docking results of top 100 hits and their pharmaceutical usage.

Sr. No.	Database ID	Compound Name	Uses of drugs	Mol. Weight (Da)	Docking score (kcal/mol)	Glide emodel (kcal/mol)
1.	DB08818	Hyaluronic acid	For the treatment of joint disorders and eye-related problems	776.649	−13.54	−83.935
2.	DB00284	Acarbose	Anti-diabetic	645.608	−12.181	−62.573
3.	DB03615	Ribostamycin	Antibiotic; Anti-HIV	454.473	−11.845	−58.629
4.	DB00104	Octreotide	For treatment of acromegaly	1019.25	−11.162	−98.49
5.	DB01421	Paromomycin	For the treatment of acute and chronic intestinal amebiasis	615.629	−11.159	−78.346
6.	DB01698	Troxerutin	Antioxidant	610.518	−11.122	−95.085
7.	DB00479	Amikacin	Antibiotic	585.602	−10.966	−72.087
8.	DB01172	Kanamycin	Antibiotic	484.499	−10.928	−58.924
9.	DB00452	Neomycin	Antibiotic	614.644	−10.071	−73.753
10.	DB04846	Celiprolol	Vasodilator	379.501	−9.83	−63.781
11.	DB01204	Mitoxantrone	Anti-neoplastic, for treating multiple sclerosis	444.481	−9.732	−81.091
12.	DB13074	Macimorelin	Ghrelin memetic, for treating adult growth hormone deficiency	474.565	−9.326	−92.817
13.	DB01193	Acebutolol	For treating hypertension and cardiac arrythmia	336.426	−9.184	−57.125
14.	DB11190	Pantethine	For lowering blood cholesterol and triglycerides	554.721	−9.076	−81.72
15.	DB13270	Dibekacin	Antibiotic	451.521	−9.009	−59.594
16.	DB08995	Diosmin	For treating hemorrhoids, and chronic venous diseases	608.545	−8.904	−78.572
17.	DB00560	Tigecycline	Antibiotic	585.649	−8.729	−73.398
18.	DB00803	Colistin	Antibiotic	1155.455	−8.699	−105.537
19.	DB09146	Iron sucrose	For treating iron deficiency	866.546	−8.08	−41.733
20.	DB00449	Dipivefrin	Prodrug of adrenaline, used to control-intra ocular pressure in open eye glaucoma	351.437	−8.51	−59.081
21.	DB00684	Tobramycin	Antibiotic	467.514	−9.834	−60.025
22.	DB08816	Ticagelor	Platelet aggregation inhibitor	522.568	−8.468	−78.186
23.	DB00997	Doxorubicin	Antibiotic	543.519	−8.59	−54.811
24.	DB00581	Lactulose	Laxative agent for treating chronic constipation	342.296	−8.248	−48.27
25.	DB00287	Travoprost	For treating ocular hypertension	500.548	−8.233	−64.479
26.	DB00445	Epirubicin	Anti-tumor effect	543.519	−8.219	−71.773
27.	DB04465	Lactose	Used as nutrient and in medical preparations	342.296	−8.125	−45.437
28.	DB01177	Idarubicin	Antineoplastic	497.494	−8.156	−62.355
29.	DB08916	Afatinib	For treating metastatic non-small cell lung cancer	485.938	−8.097	−86.799
30.	DB00118	Ademetionine	Anti-inflammatory, for treating chronic liver diseases	398.44	−8.073	−56.482
31.	DB00938	Salmeterol	For treating asthma and chronic obstructive pulmonary disease	415.566	−8.069	−64.203
32.	DB01082	Streptomycin	Antibiotic	581.574	−10.415	−62.467
33.	DB09050	Ceftolozane	Antibacterial	666.69	−9.869	−94.804
34.	DB06791	Lanreotide	For treating acromegaly and carcinoid syndrome	1096.33	−9.827	−86.499
35.	DB14568	Ivosidenib	For treating acute myeloid leukemia	582.97	−8.657	−76.875
36.	DB06663	Pasireotide	For treating Cushing's syndrome	1047.206	−8.515	−89.032
37.	DB00314	Capreomycin	Antibiotic	1321.412	−8.382	−74.787
38.	DB06267	Udenafil	For treating erectile dysfunction	516.656	−8.048	−81.068
39.	DB08868	Fingolimod	For treating multiple sclerosis	307.471	−8.034	−63.569
40.	DB00140	Riboflavin	Neutraceutical	376.364	−8.01	−64.756
41.	DB11842	Angiotensin II	Vasoconstrictor	1046.179	−7.913	−100.789
42.	DB09026	Aliskiren	Renin inhibitor, for treating hypertension	551.758	−7.927	−73.187
43.	DB00798	Gentamycin	Antibiotic	477.595	−7.913	−49.219
44.	DB11986	Entrectinib	For treating ROS-1 positive non-small cell lung cancer and NTRK gene fusion positive solid tumors	560.65	−7.855	−81.876
45.	DB00481	Ralofixene	Anti-estrogen, for prevention and treatment of osteoporosis, corticosteroid-induced bone loss, and invasive breast cancer	473.583	−7.799	−71.274
46.	DB01232	Saquinavir	HIV protease inhibitor	670.841	−7.798	−77.88
47.	DB00623	Fluphenazine	For treating psychosis	437.522	−7.793	−67.712
48.	DB01076	Atorvastatin	For treating dyslipidemia and preventing cardiovascular diseases	558.64	−7.787	−78.135
49.	DB12615	Plazomycin	Antibacterial used for treatment of complicated Urinary tract infections.	592.691	−9.778	−72.324
50.	DB13265	Hexobendine	Vasodilator	592.686	−7.744	−76.055
51.	DB01095	Fluvastatin	Statin used for preventing cardiovascular diseases	411.466	−7.721	−64.343
52.	DB11827	Ertugliflozin	For improving glycemic control in type 2 diabetes	436.89	−7.706	−60.905
53.	DB00211	Midodrine	Vasoconstrictor, for treating hypotension	254.282	−7.689	−49.714

(*continued*)

Table 2. Continued.

Sr. No.	Database ID	Compound Name	Uses of drugs	Mol. Weight (Da)	Docking score (kcal/mol)	Glide emodel (kcal/mol)
54.	DB01598	Imipenem	Antibacterial	299.346	−7.676	−50.15
55.	DB00195	Betaxolol	For treating hypertension	307.428	−7.67	−49.774
56.	DB00512	Vancomycin	Antibacterial	1449.254	−7.669	−90.77
57.	DB08893	Mirabegron	For treating overactive bladder	396.506	−7.544	−66.775
58.	DB09335	Alatrofloxacin	Antibiotic	558.518	−7.538	−83.603
59.	DB09082	Vilanterol	For treating COPD and asthma	486.43	−7.536	−75.659
60.	DB01118	Amiodarone	Antiarrhythmic	645.312	−7.532	−64.154
61.	DB09330	Osimertinib	For treatment of metastatic EGFR-T790M mutation positive non − small cell lung cancer (NSCLC).	499.619	−7.503	−86.439
62.	DB01203	Nadolol	Used to lower blood pressure.	309.401	−7.5	−54.254
63.	DB06717	Fosaprepitant	Used to prevent nausea associated with chemotherapy treatment.	614.407	−7.479	−80.068
64.	DB01195	Flecainide	Anti-arrhythmic agent	414.343	−7.452	−58.535
65.	DB00955	Netilmicin	Aminoglycoside antibiotic	475.587	−7.442	−53.689
66.	DB01297	Practolol	Treatment of cardiac arrhythmia	266.336	−7.426	−45.129
67.	DB00176	Fluvoxamine	Anti-depressant	318.34	−7.424	−50.184
68.	DB00738	Pentamidine	Anti-protozoal agent	340.42	−7.409	−54.139
69.	DB08874	Fidaxomicin	Anti-biotic used for treatment of diarrhoea	1058.039	−7.392	−67.174
70.	DB00722	Lisinopril	Used to treat hypertension, heart failure and myocardial infarction.	405.488	−7.378	−58.31
71.	DB11712	Tezacaftor	Used as Cystic Fibrosis membrane conductance regulator	520.505	−7.367	−67.889
72.	DB01182	Propafenone	Anti-arrhythmia agent	341.444	−7.355	−61.246
73.	DB11263	Polydatin	Possesses anti-inflammatory, immune-regulatory, anti-oxidative and anti-tumor activities.	390.388	−7.767	−58.642
74.	DB06193	Pixantone	Used in treatment of relapsed or refractory non-Hogkin's Lymphoma (NHL)	325.372	−7.329	−62.038
75.	DB06736	Aceclofenac	Non-steroildal anti-inflammatory drug.	354.18	−7.307	−47.903
76.	DB01098	Rosuvastatin	Lipid lowering drug used to lower risk of cardiovascular disease.	481.538	−7.293	−69.399
77.	DB11155	Triclocarban	Anti-bacterial agent effective against Gram positive bacteria.	315.58	−7.27	−46.515
78.	DB00224	Indinavir	Antiviral drug used HIV-type I	613.789	−7.245	−87.086
79.	DB01062	Oxybutynin	Anti-cholinergic medication	357.486	−7.222	−57.409
80.	DB06441	Cangrelor	Reversible P2Y12 inhibitor for patients undergoing percutaneous coronary intervention (PCI)	776.35	−7.204	−99.813
81.	DB13274	Micronomicin	Aminoglycoside antibiotic	463.576	−7.202	−52.655
82.	DB08932	Macitentan	Used by people with pulmonary arterial hypertension.	588.273	−7.201	−79.928
83.	DB06608	Tafenoquine	Used for treatment and prevention of relapse in vivax malaria.	463.501	−7.189	−62.476
84.	DB00694	Daunorubicin	Used for treatment of leukemia and other neoplasms.	527.52	−8.15	−55.99
85.	DB09092	Xanthinol	Used as a vasodilator	311.342	−7.174	−49.809
86.	DB00358	Mefloquine	Anti-malarial drug	378.312	−7.168	−51.161
87.	DB01624	Zuclopenthixol	Anti-psychotic agent	400.965	−7.145	−62.147
88.	DB08860	Pitavastatin	Lipid lowering drug	421.461	−7.129	−63.977
89.	DB11732	Lasmiditan	Used for termination of migranes.	377.367	−7.104	−54.791
90.	DB00410	Mupirocin	Broad spectrum antibiotic	500.622	−7.099	−64.487
91.	DB12783	Benserazide	Given in combination with Levadopa to minimize side-effects of Levadopa in Parkinson's disease therapy	257.246	−7.094	−48.452
92.	DB08882	Linagliptin	DPP-4 inhibitor used for treatment of type II diabetes.	472.542	−7.092	−63.844
93.	DB00188	Bortezomib	Used for treatment of relapsed myeloma and mantle cell lymphoma.	384.237	−7.081	−68.167
94.	DB01030	Topotecan	Anti-neoplastic agent used to treat ovarian cancer.	421.446	−7.076	−57.118
95.	DB01396	Digitoxin	Used to treat heart failure	764.939	−7.066	−67.588
96.	DB13532	Cyclopenthiazide	Diuretic with anti-hypersentitive properties.	379.87	−7.062	−55.037
97.	DB00675	Tamoxifen	Used to treat estrogen receptor positive breast cancers.	371.515	−7.052	−59.058
98.	DB00961	Mepivacaine	Local anaesthetic	246.348	−7.115	−37.177
99.	DB06292	Dapagliflozin	Used for managing diabetes mellitus type 2	408.873	−7.034	−56.858
100.	DB00606	Cyclothiazide	Diuretic used for treatment of edemaassociated with congestive heart failure, hepatic cirrhosis and corticosteroid and estrogen therapy	389.878	−7.03	−57.596

Table 3. A summary of XP-docking results of selected approved drugs in clinical trials for COVID-19.

Sr. No.	Database ID	Compound name	Uses of drugs	Molecular weight (Da)	Docking score (kcal/mol)	Glide emodel (kcal/mol)
1.	DB00811	Ribavirin	Antiviral	244.205	−6.813	−49.566
2.	DB01601	Lopinavir	Antiviral	628.801	−6.119	−81.525
3.	DB00207	Azithromycin	Antibiotic	748.985	−5.636	−42.186

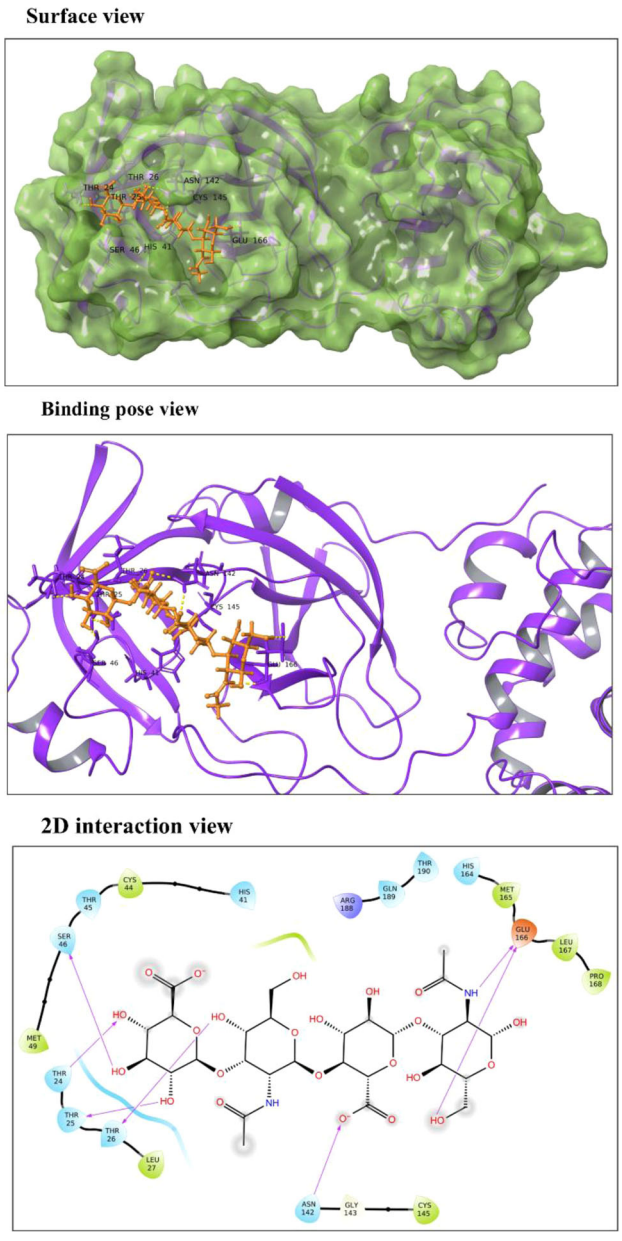

Figure 2. Molecular interaction of Hyaluronic Acid (HA) at M^{pro} active site 1. In surface and binding pose views, ligand is represented with orange color and interacting residues are labeled. In 2D interaction view, arrows correspond to H-bonds formed between HA and M^{pro}.

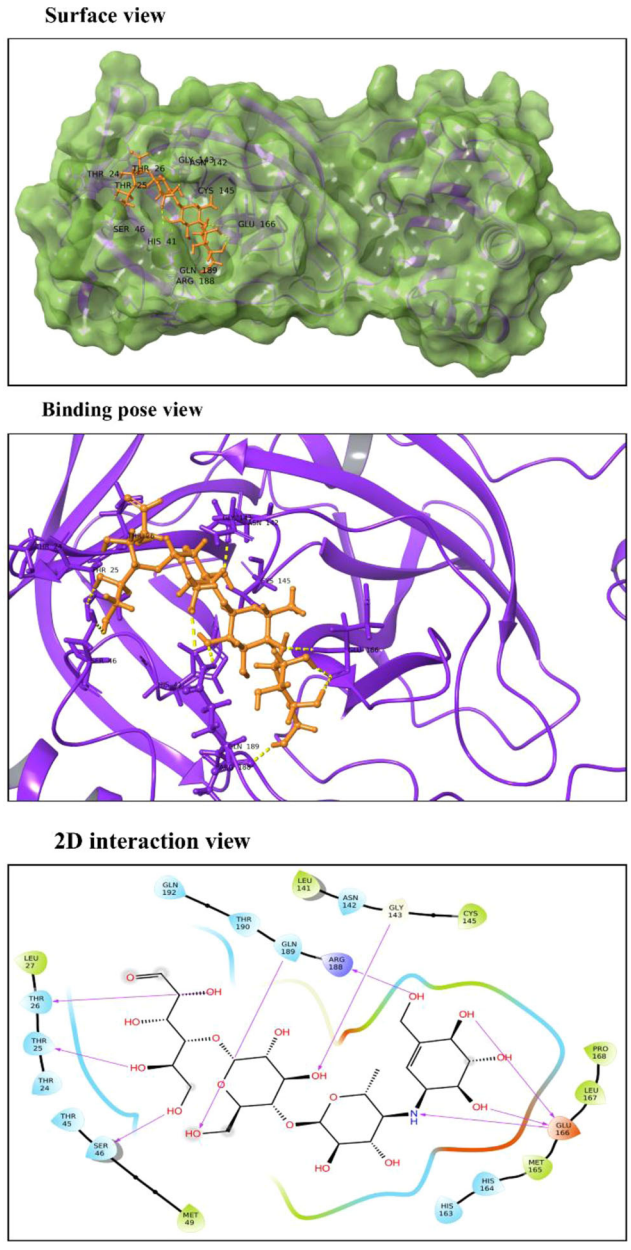

Figure 3. Molecular interaction of Acarbose with M^{pro} active site 1. In surface and binding pose views, ligand is represented with orange color and interacting residues are labeled. In 2D interaction view, arrows correspond to H-bonds formed between Acarbose and M^{pro}.

type 1 and type 2, Influenza Virus A/H1N1 and Porcine Parvovirus in a nonspecific manner (Cermelli et al., 2011).

Acarbose: Also known as acarbosa and acarbosum, it is an approved oral drug prescribed to Diabetes Mellitus type II patients. Acarbose is observed to interact with Thr25, Thr26, Ser46, Gly143, Glu166 and Gln189 residues of M^{pro} (Figure 3). These residues are a part of domains I and II which constitute β-barrels enclosing the active site. It binds to Mpro with a significant docking score of −12.181 kcal/mol and binding energy of −45.54 kcal/mol. It reduces the amount of glucose in blood by delaying the absorption of carbohydrates. Acarbose is a complex oligosaccharide that works by inhibiting the α-amylase and glycosidase enzymes of pancreatic and intestinal cells, thereby preventing the hydrolysis of poly-carbohydrates to glucose (DiNicolantonio et al., 2015).

Amikacin: According to our results, docking score of drug Amikacin is −10.966 kcal/mol, and binding energy of −52.25 kcal/mol. Drug-interaction view exposes the interaction of Amikacin

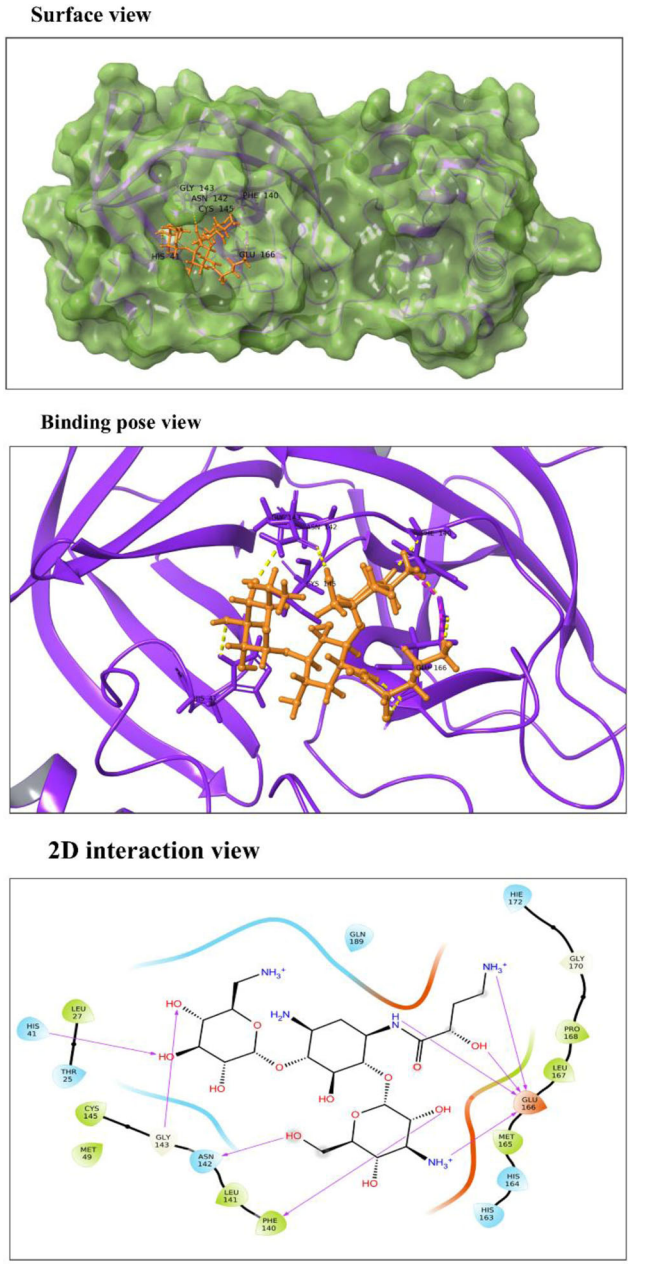

Figure 4. Molecular interaction of Amikacin with M^{pro} active site 1. In surface and binding pose views, ligand is represented with orange color and interacting residues are labeled. In 2D interaction view, arrows corresponds to H-bonds formed between Amikacin and M^{pro}.

with His41 residue of M^{pro} which is one of the two residues of catalytic dyad conserved in catalytics site of coronaviruses (Figure 4). It also interacts with Phe140, Asn142, Gly143 and Glu166 residues present in domain II. It is a well-known broad-spectrum antibacterial drug prescribed for the treatment of life-threatening gram-negative bacterial infections (Ramirez & Tolmasky, 2017; Tamma et al., 2012). Recently in 2018, Amikacin liposome inhalation suspension (ALIS, Arikayce®) is approved for treating patients suffering from mycobacterium avium complex lung diseases therapy (Shirley, 2019).

Ribostamycin: Docking score of Ribostamycin on SARS-CoV-2 protease is estimated to be −11.845 kcal/mol with a glide binding energy of −36.45 kcal/mol (Table 2). The M^{pro}-Ribostamycin complex is stabilized by five H-bonds formed between Phe140, Leu141, His164 and Glu166 residues of protease and the compound (Figure 5(a)). It is an aminoglycosidic anti-bacterial compound but is demonstrated to have an antiviral activity against HIV-1 as well (Ennifar et al., 2006). Our previous in-silico study has also reported nsp2 cysteine protease of chikungunya virus as one of the targets of Ribostamycin (Kumar et al., 2019).

Octreotide: The long-acting octapeptide has a cyclic structure mimicking to that of natural hormone somatostatin. Due to similar pharmacologic properties to endogenous hormone, it is a potent inhibitor of growth hormone, luteinizing hormone, insulin and glucagon (Battershill & Clissold, 1989; McKeage et al., 2003). Our docking analysis has given it a very significant binding score of −11.162 kcal/mol. The drug form H-bonds with Thr26, Ser46, Gly143, Leu141, Glu166 and Gln189 residues and a salt bridge interaction with Glu166 of protease with a binding energy of −66.41 kcal/mol (Figure 5(b)). It is recommended for the treatment of acromegaly and thyrotrophinomas (Battershill & Clissold, 1989; McKeage et al., 2003). As an analogue of somatostatin, Octreotide has been reported to bind with somatostatin receptor and exert its influence on downstream signaling (Hofland & Lamberts, 1996). In a direct way, this drug has not been reported against any of the viral infection, as per our knowledge. However, several octapeptide substrates have been functionally characterized against Nsp3 helicase protein of all serotypes of Dengue virus (Li et al., 2005).

Paromomycin: It is prescribed as a first line drug for the treatment of intestinal amebiasis and visceral leishmaniasis (Davidson et al., 2009; Shalev-Benami et al., 2017). In our docking study, it is observed to interact via H-bonds with Phe140, Leu141, Asn142, Glu166, Gln189 and Thr190 residues of M^{pro} and shows a powerful docking score of −11.159 kcal/mol (Figure 5(c)). Furthermore, the stability of complex is increased by a salt bridge interaction between $NH3^{+}$ and Glu166 residue (Details of binding parameters are given in Table 2).

Lopinavir: According to our docking results (docking score of −6.119 kcal/mol), Lopinavir-protease complex is stabilized by two H-bonds formed by Thr25, and Glu166 amino acids of protease with the drug (Table 3). In conjunction with H-bonds, a Pi-Pi stacking interaction with His41 further increases the stability of complex upto −46.98 kcal/mol of binding energy (Figure 6(a)). It is an FDA-approved peptidomimetic compound containing a hydroxyethylene scaffold that mimics the peptide bond. Co-formulated capsules with Ritonavir, marketed as Kaletra® are widely used for the treatment of HIV (Chandwani & Shuter, 2008). As an anti-retroviral drug, Lopinavir in combination with Ritonavir is demonstrated to suppress viral replication.

Azithromycin: It shows a docking score of −5.636 kcal/mol and is observed to form a single H-bond with Leu141 in addition with a salt bridge interaction between NH^{+} and Glu166 residue (Figure 6(b)). The M^{pro}-Azithromycin complex exhibits a binding energy equivalent to −46.25 kcal/mol. Approved by FDA in 1991, it is a broad-spectrum antibiotic drug

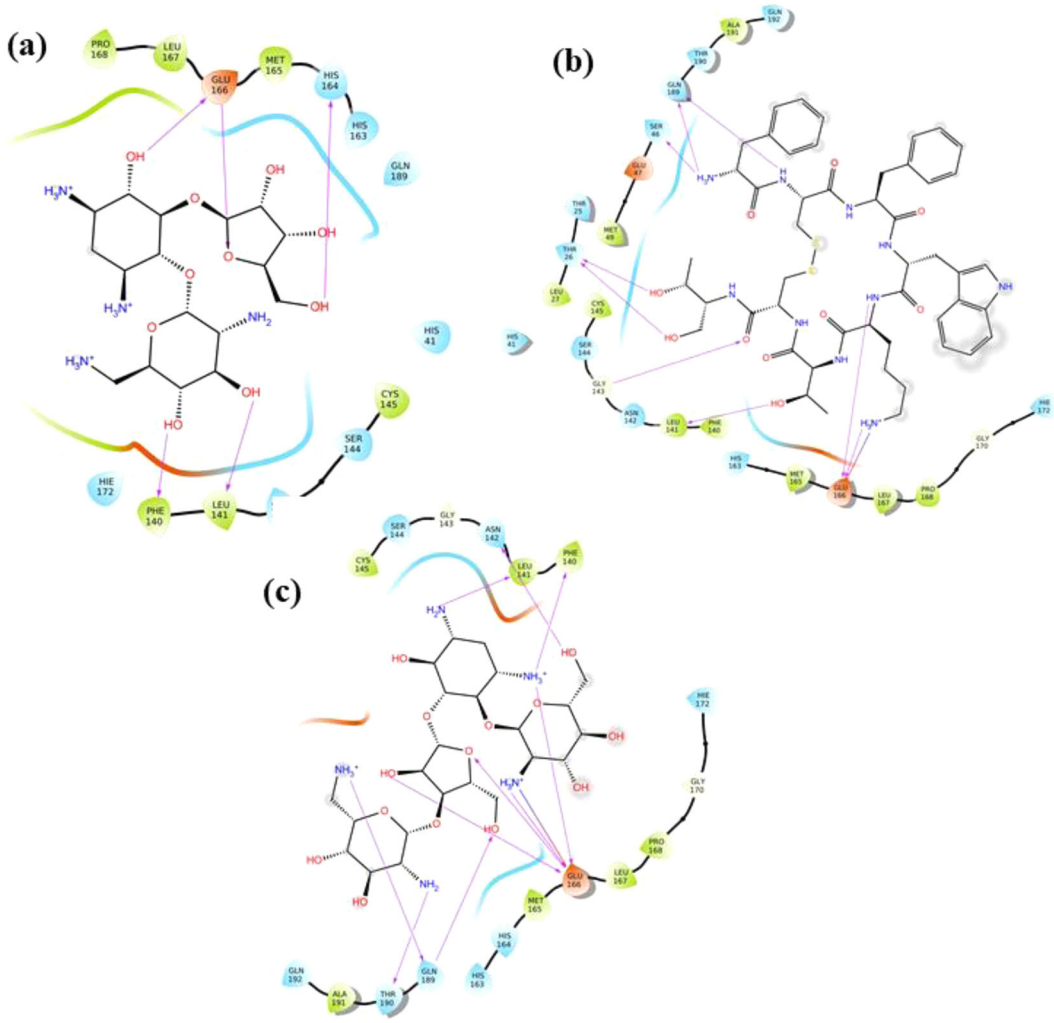

Figure 5. 2D Molecular interaction views of (a) Ribostamycin, (b) Octreotide and (c) Paromomycin with M^{pro}. Arrows correspond to H-bonds formed by the drug molecule with residues of M^{pro}.

administered orally during respiratory, enteric, and genitourinary infections (Peters et al., 1992). As a macrolide having a 15-membered ring, it shows bacteriostatic activity against Gram-negative as well as Gram-positive bacteria. Although considered safe for use during pregnancy, it occasionally causes diarrhea in breast-feeding infants (McMullan & Mostaghim, 2015; Peters et al., 1992). As mentioned above, presently, Azithromycin is in clinical trials along with Hydroxychloroquine for the treatment of COVID-19 infection ('Evaluation of the efficacy of the hydroxychloroquine-azithromycin combination in the in the prevention of COVID-19 related SDRA', 2020; 'Safety and efficacy of hydroxychloroquine associated with azithromycin in SARS-CoV2 virus', 2020). However, FDA has approved it for emergency use against SARS-CoV-2.

Ribavirin: In our study, docking analysis of Ribavirin revealed a docking score equivalent to −6.813 kcal/mol (Table 3). The drug establishes H-bonds with His164, Glu166, Gln189 and Thr190 residues of SARS-CoV-2 main protease (binding energy −35.63 kcal/mol) (Figure 6(c)). It is a broad-spectrum FDA-approved antiviral drug used against a number of DNA and RNA viruses including respiratory syncytial virus, parainfluenza virus and hepatitis C virus (Krilov, 2001; Reddy et al., 2009). It is a synthetic guanosine analogue which interfers with viral RNA synthesis. Administered orally, Ribavirin is prescribed in combination with pegylated interferon-α2 for treating hepatitis C virus infection (Loustaud-Ratti et al., 2016; Reddy et al., 2009). On the basis of its *in-vitro* efficacy against SARS-CoV and MERS-CoV, it is being clinically tested on COVID-19 patients (Khalili et al., 2020).

The catalytic site of M^{pro} and nearby residues in contact such as Phe140, Leu141, His164, Glu166, Glu189 are observed to be important for binding of these drugs. Therefore out of 100 shortlisted drugs, we have chosen HA, Acarbose, and Amikacin on the basis of their high docking scores and molecular interactions with catalytic site and nearby residues of M^{pro}. Additionally, binding stability of the drug Lopinavir is also investigated through molecular simulation.

Molecular dynamics simulation

The stability of protein-ligand complexes with respect to protein conformation is determined by MD simulations. In general, a small deviation in protein conformation during the course of simulation indicates a stable protein structure. We analyzed the atomic distance and fluctuation in protein upon

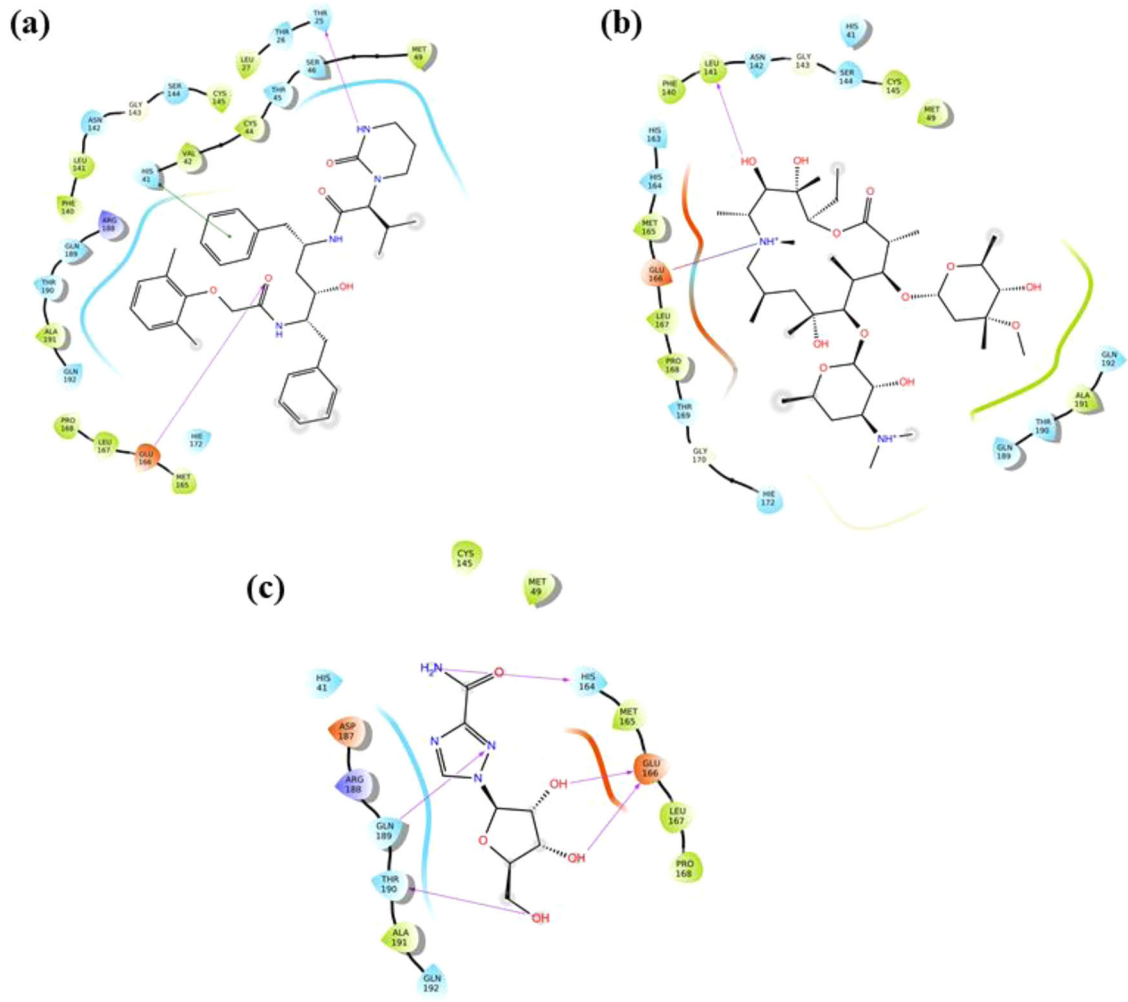

Figure 6. 2D Molecular interaction views of (a) Lopinavir, (b) Azithromycin and (c) Ribavirin with M^{pro}. Arrows, blue-red straight line and green straight line corresponds to H-bonds, salt bridge and pi-pi interactions formed between the drug molecules with residues of M^{pro}.

binding of drug molecule at the active site 1 of M^{pro}. Acarbose, HA, Amikacin and Lopinavir complexes with M^{pro} are monitored for 500 ns using our in-house high-performance cluster facility.

Assessment of root mean square deviation (RMSD), root mean square fluctuation (RMSF) and radius of gyration (Rg)

The average RMSD of 6LU7-HA, 6LU7-Acarbose, 6LU7-Amikacin and 6LU7-Lopinavir complex is observed to be 0.42 nm, 0.31 nm, 0.37 nm and ~0.4 nm, respectively. 6LU7-HA complex attains a stable conformation till 15 ns, after which deviation starts increasing and the complex become unstable near 400 ns. For 6LU7-Acarbose, RMSD keeps on fluctuating between 0.2 nm and 0.3 nm during the entire simulation period. Nonetheless, these RMSD values are still much lower than that of other two compounds 6LU7-HA and 6LU7-Amikacin (Figure 7). The RMSF plot identifies flexible regions in protein-ligand complexes. Residues with low RMSF values indicate its contribution to the structured regions, while higher residual fluctuation indicates the presence of unstructured regions such as loops and turns in protein. The binding of an inhibitor or druggable compound through one or more stable bonds, however, reduces the fluctuation in residues. As illustrated in Figure 8, Lopinavir bound protease complex is observed to have higher fluctuating (0.4–0.6 nm) peaks showing less stable binding. Contrary to this, 6LU7-Acarbose, 6LU7-HA and 6LU7-Amikacin complexes are showing less fluctuations (between 0.1 to 0.3 nm). Similarly, Rg for 6LU7-HA and 6LU7-Acarbose are observed to be 2.18 nm and 2.17 nm, respectively. For 6LU7-Amikacin, and 6LU7-Lopinavir complexes, respective mean Rg values are calculated to be 2.2 nm and 2.16 nm. Graphs in Figure 9 illustrate the Rg for complex of M^{pro} (6LU7) with HA, Amikacin, Acarbose, and Lopinavir. The time-dependent trace of Rg is stable for HA, and Acarbose throughout the simulation. In case of Amikacin, the complex is showing higher fluctuation between 2.15 nm to 2.25 nm beyond 275 ns. Although, 6LU7-Lopinavir, at initial stage of simulation acquires a high Rg upto 2.25 nm, however, beyond 60 ns itdecreases and becomes stable till 425 ns.

Assessment of principle component analysis (PCA) and solvent solvent accessible surface area (SASA)

Binding of ligand induces local as well as global fluctutaions in protein structure that are hard to distinguish. In order to identify the simultaneously occurring conformational

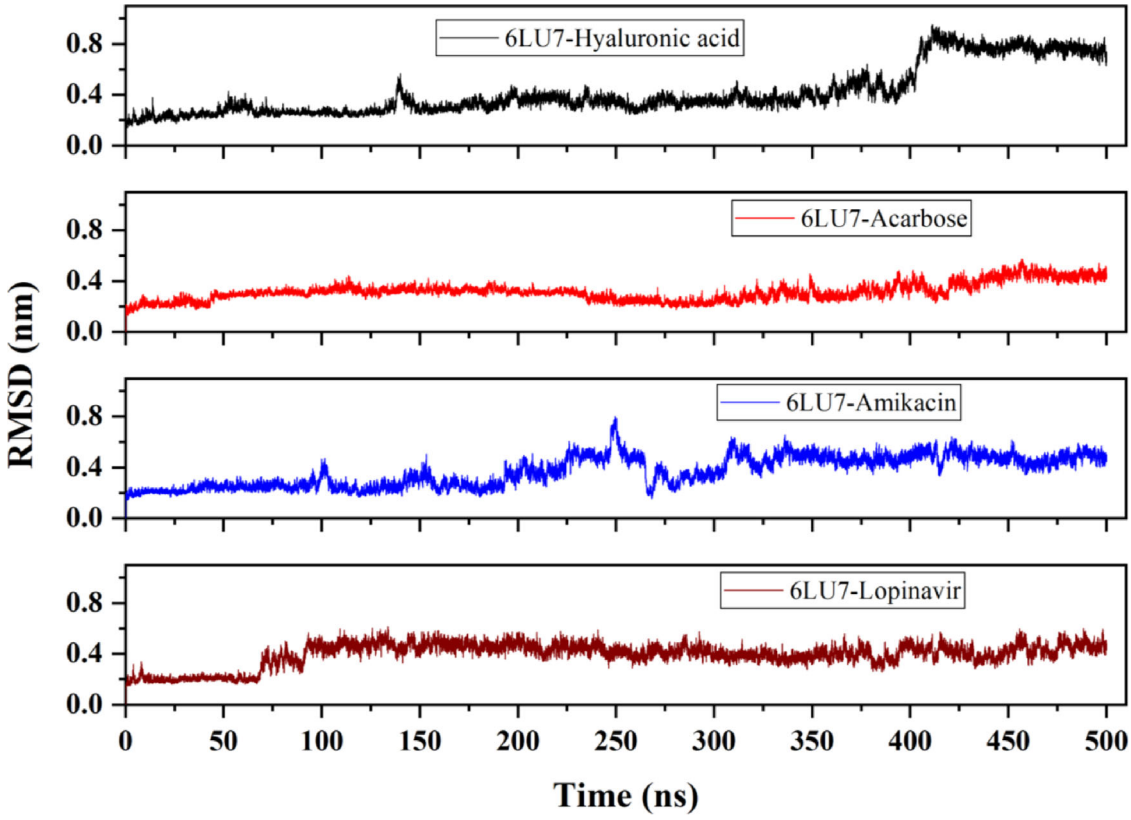

Figure 7. Evaluation of root mean square deviation (RMSD) from molecular dynamic trajectory of M^{pro} (6LU7) in complex with HA, Acarbose, Amikacin and Lopinavir.

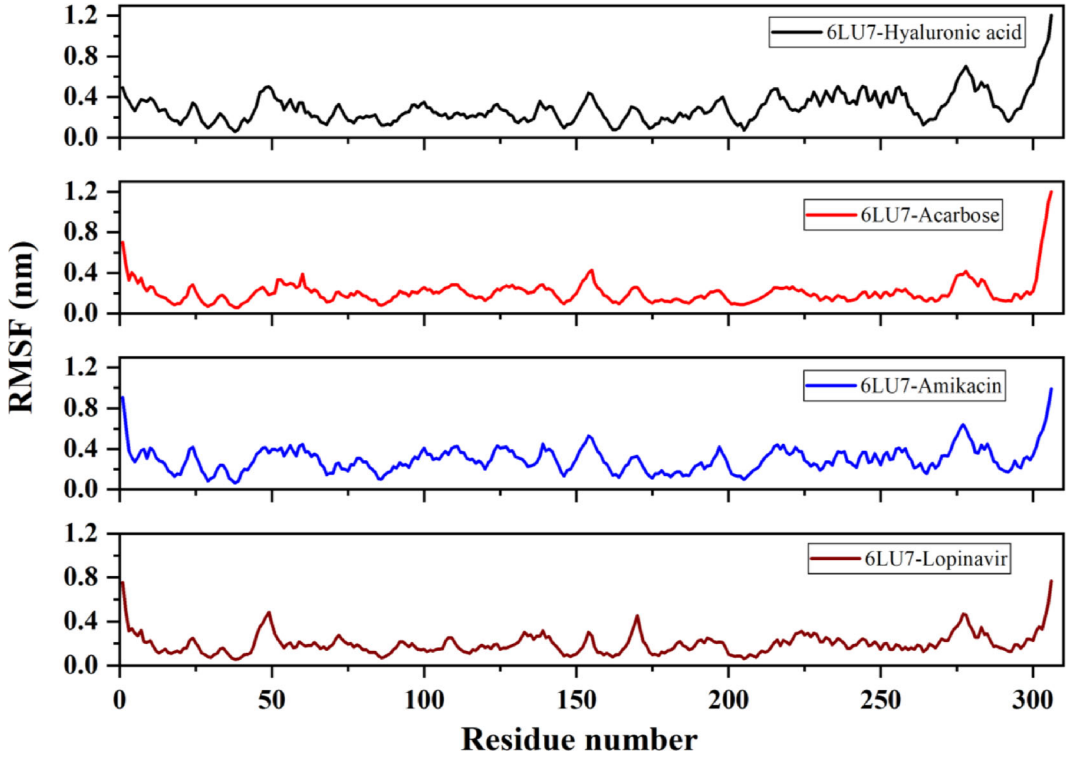

Figure 8. Evaluation of root mean square fluctuation (RMSF) of M^{pro} (6LU7) residues upon binding with HA, Acarbose, Amikacin and Lopinavir.

changes, PCA is performed for C-α atoms of protease. It is a multivariate statistical technique which builds a co-varinace or correlation matrix for methodically calculating eigenvectors and eigenvalues. PCA generates eigenvectors which represents the reduced collective atomic motions in protein structure (David & Jacobs, 2014).

The effect of ligand stabilization on protein structure is shown in Figure 10 where PC1 and PC2 majorly contributes

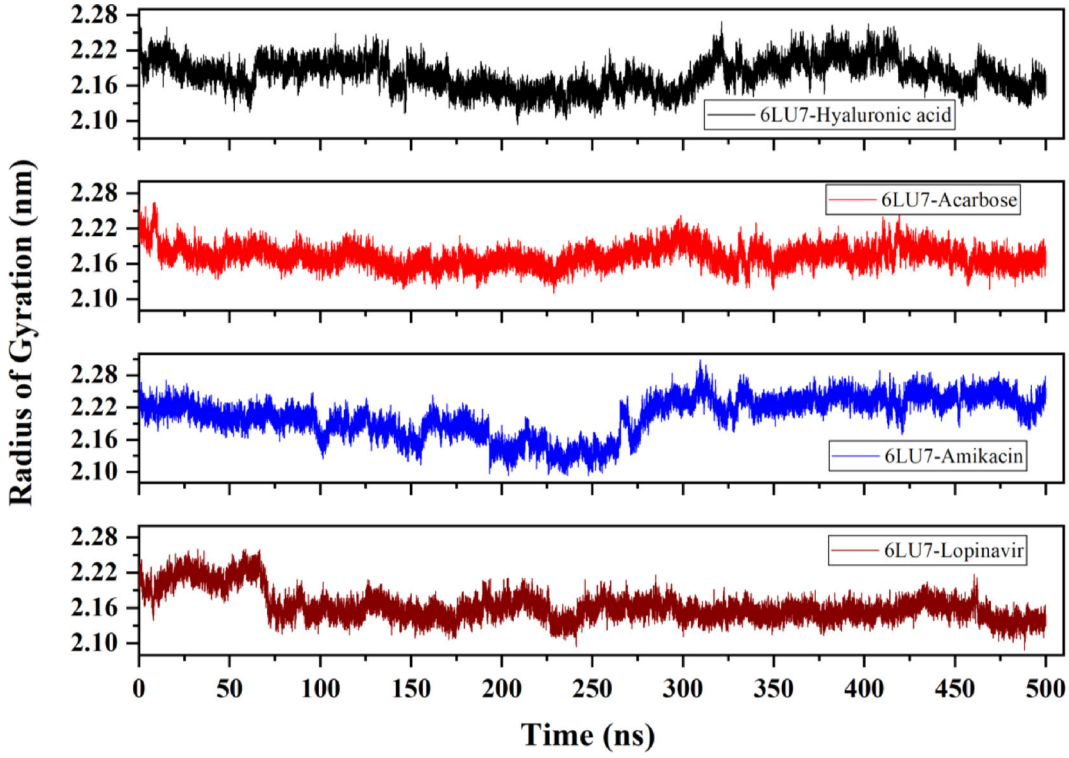

Figure 9. Evaluation of protein structure compactness through radius of gyration (Rg) for HA, Acarbose, Amikacin and Lopinavir bound M^{pro} (6LU7).

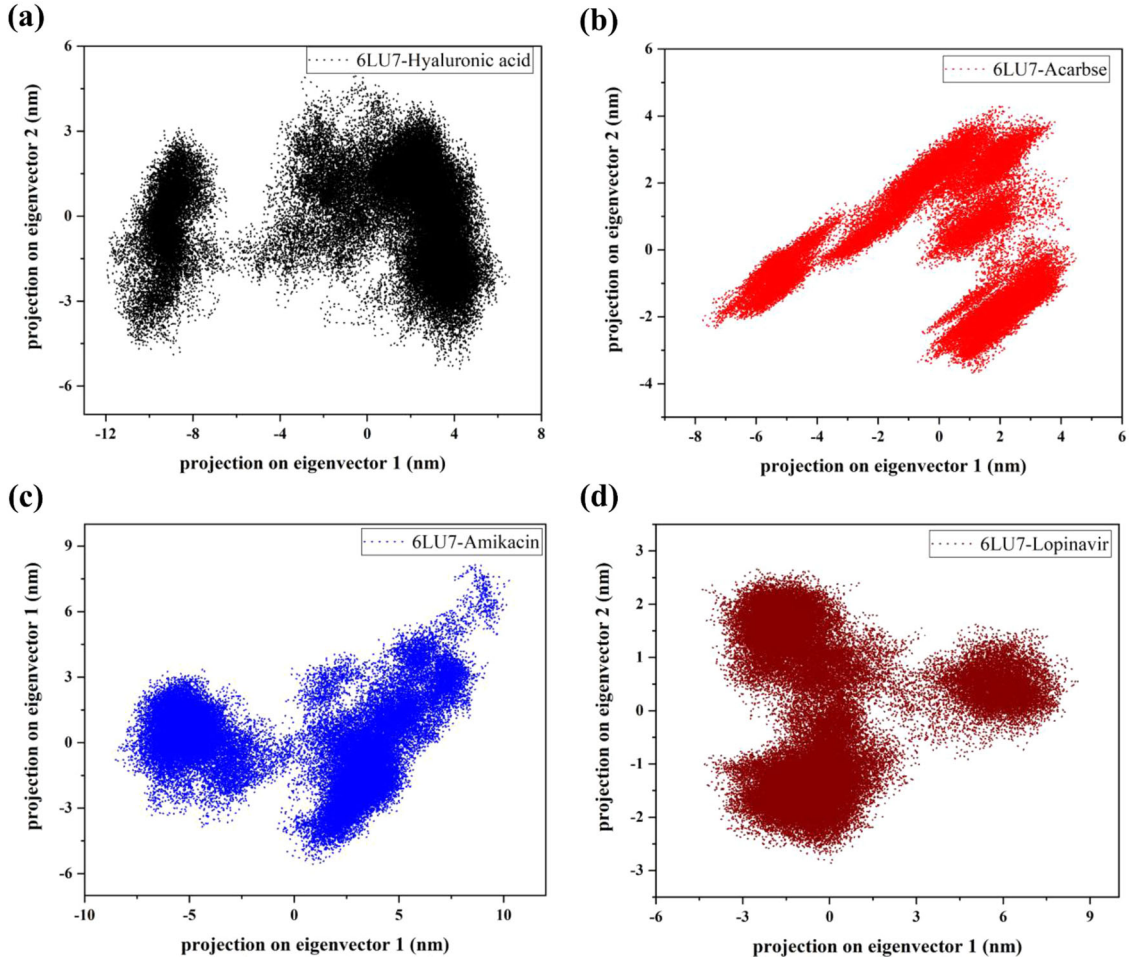

Figure 10. Depiction of principal component analysis (PCA). Projection on eigenvector 1 against eigenvector 2 for HA, Acarbose, Amikacin and Lopinavir bound M^{pro} (6LU7).

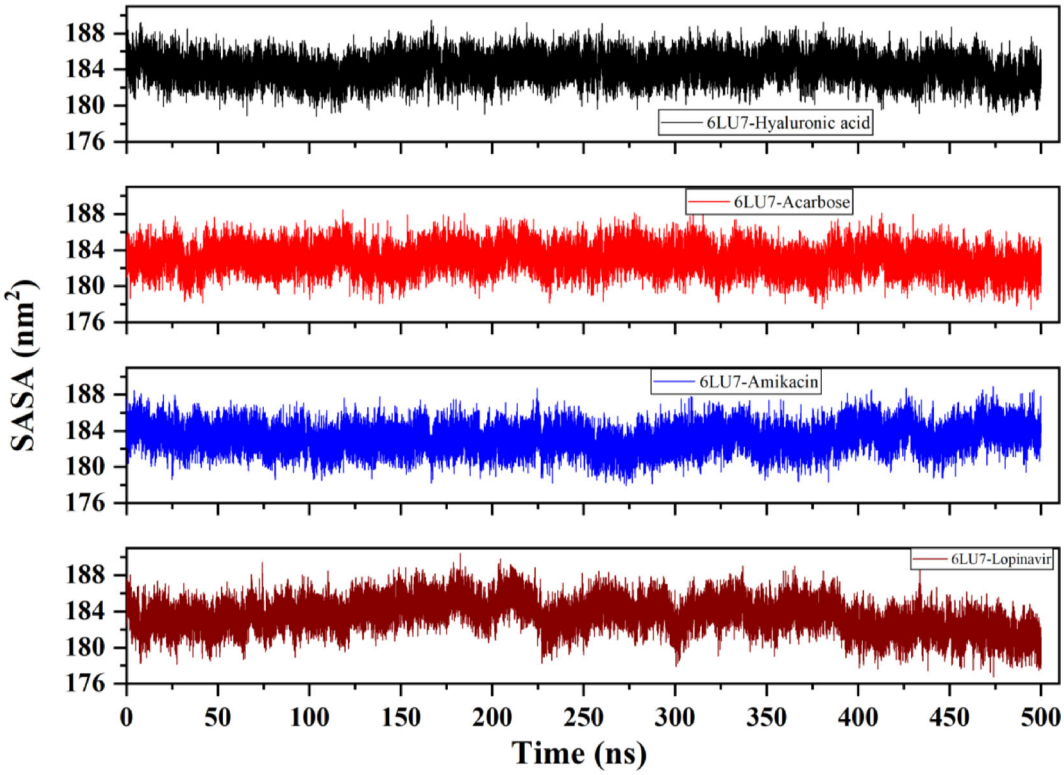

Figure 11. Evaluation of solvent accessible surface area (SASA) of M^{pro} (6LU7) upon binding with HA, Acarbose, Amikacin and Lopinavir. Acarbose and HA bound M^{pro} have attained more stable states during simulation.

to global conformations of 6LU7-ligand complexes. As observed in the analysis, dense clusters are formed in all drug bound forms of protease but Amikacin and HA have higher range from −10 to 10 nm and −12 to 6 nm, respectively. However, Lopinavir has shown stable clusters with a range of −5 to 5 nm and similarly, the second top hit drug, Acarbose is observed to form clusters of stable positions (−7 to 2 nm). This indicates that binding of Acarbose has reduced the global conformational changes occurring in M^{pro} while HA has slightly higher values, may be due to little fluctuation in the last 100 ns period of simulation.

Hydrophobic force deriving protein folding results in formation of hydrophobic cores with hydrophilic residues assembling near the surface of a protein structure. Binding of ligand can significantly affect the SASA of a protein, in which overall differences related to ligand-induced stability in complex are frequently estimated. Therefore, we also investigated the SASA parameter in this study. Figure 11 depicts the SASA values of C-α atoms of M^{pro} complexes upon binding with screened drugs. In correlation with RMSD, RMSF and Rg analysis, 6LU7-Lopinavir has a gradually increasing surface area (188 nm^2) till 200 ns illustrating higher protein surface exposure. The complex is then observed to be fluctuating a little which again decreases after 400 ns to 178 nm^2. However, Acarbose and HA has a stable trend of SASA values than Amikacin bound M^{pro} with an average value of 184 nm^2 but Amikacin experiences higher fluctuations after 250 ns. This also confirms that the top screened drugs Acarbose and HA have gained firm binding with M^{pro}.

Numerous attempts of drug repurposing have been made against SARS-CoV-2 M^{pro} enzyme. In one of the reports, Sang *et al*. explored inhibitory effect of approved anti-HIV drugs, which have shown stable interactions with residues Met49, Leu141, Cys145, Met165, Pro168 and Glu189 of M^{pro} (Sang et al., 2020). In another study, synergistic effect of Lopinavir, Oseltamivir and Ritonavir are investigated. These drugs are stabilized by interaction with Lue287, Tyr101, Asp33, His41, Asn142 and Glu166 residues of M^{pro} (6LU7) (Muralidharan et al., 2020). Khan et al. showed stable binding of two compounds Paritaprevir and Raltegravir with SARS-CoV-2 M^{pro} (shows multiple interactions with Thr24, Ser46, Leu50, Asn142, Cys145 and Pro168) (Khan et al., 2020). Another approach of using combination of drugs is frequently observed to be highly effective. Lopinavir-Ritonavir complex shows a stable binding affinity of −10.6 kcal/mol with SARS-CoV-2 M^{pro}. The combination drug is found to interact with one of the catalytic dyad residue His41, and further His164, Glu166, Arg188 and Gln192 of M^{pro} active site (Kumar, Singh et al., 2020).

Our simulation analysis of 6LU7-HA, 6LU7-Acarbose, 6LU7-Amikacin and 6LU7-Lopinavir complex reveals stable binding of Acarbose, and HA at M^{pro} active site. Interaction of Lopinavir stabilized by multiple non-covalent bonds with catalytic as well as surrounding residues (such as Asn142 and Glu166) of M^{pro} is in line with the previously reported literature (Kumar, Singh et al., 2020; Muralidharan et al., 2020). Antiviral effects of HA against both DNA and RNA viruses are already well described (Cermelli et al., 2011). Although Amikacin and Acarbose are not much known to exert antiviral effects, however, they have shown significant docking and simulation results. Therefore, these drugs may have inhibitory potential and are need to be tested experimentally for their efficacy against SARS-CoV-2.

A study by Victorovich et al., has observed that among more than 250 nucleotide mutations (known yet), there are more number of synonymous Cytosine to Uracil transitions in ORF 1a and 1b which have caused mutational U-pressure in RNA plus strand of SARS-CoV-2 and that can not be repaired by proofread machinery of coronaviruses (Victorovich et al., 2020).

Conclusion

The current scenario of the COVID-19 pandemic urgently needs drugs to treat patients. However, at the same time, we need to understand the mechanisms or the interactions of those drugs on the molecular targets on SARS-CoV-2. In this study, we have screened the approved drugs against the M^{pro} of SARS-CoV-2 to investigate their binding efficacies and molecular interactions. We found that HA, Acarbose, Ribostamycin, Paromomycin, and Amikacin have good binding efficacy with the target. The interaction with the catalytic dyad (-His41, -Cys145) at the active site, seen in Amikacin, and Lopinavir may be responsible for inhibiting M^{pro}. Additionally, HA and Acarbose have also given the stable binding in 500 ns MD simulation time as observed from atomic distance, fluctuations and PCA. Further, the inhibition of M^{pro} may lead to the inhibition of SARS-CoV-2 replication and propagation. As elucidated, these drugs may act as potential inhibitors against COVID-19 by targeting M^{pro} of SARS-CoV-2. However, *in-vitro* validation of these identified drugs is essential to test the inhibition potency.

Authors contribution

RG, NG and GN: Conception and design. RG: review and writing of the manuscript, and study supervision. PK, TB, AK, BRG, SK: acquisition andinterpretation of data, writing of the manuscript.

Acknowledgements

All the authors would like to thank IIT Mandi for providing HPC facilities. RG would like to thank the Department of Biotechnology, Govt of India (BT/11/IYBA/2018/06). TB is grateful to the Department of Science and Technology for INSPIRE fellowship. PK, SK, AK, and BRG are supported by MHRD fellowship, Govt. of India.

Disclosure statement

All authors declare that there is no financial or any other type of competing interest.

Funding

This work was supported by Department of Biotechnology, Ministry of Science and Technology.

ORCID

Prateek Kumar http://orcid.org/0000-0001-7392-5045
Taniya Bhardwaj http://orcid.org/0000-0002-7226-6348
Neha Garg http://orcid.org/0000-0003-2227-8292
Rajanish Giri http://orcid.org/0000-0002-2046-836X

References

Aarthy, M., Kumar, D., Giri, R., & Singh, S. K. (2018). E7 oncoprotein of human papillomavirus: Structural dynamics and inhibitor screening study. Gene, *658*, 159–177. https://doi.org/10.1016/j.gene.2018.03.026

Anand, K., Ziebuhr, J., Wadhwani, P., Mesters, J. R., & Hilgenfeld, R. (2003). Coronavirus main proteinase (3CLpro) structure: Basis for design of anti-SARS drugs. *Science*, *300*(5626), 1763–1767. https://doi.org/10.1126/science.1085658

Ashburn, T. T., & Thor, K. B. (2004). Drug repositioning: Identifying and developing new uses for existing drugs. *Nature Reviews. Drug Discovery*, *3*(8), 673–683. https://doi.org/10.1038/nrd1468

Battershill, P. E., & Clissold, S. P. (1989). Octreotide. A review of its pharmacodynamic and pharmacokinetic properties, and therapeutic potential in conditions associated with excessive peptide secretion. Drugs, *38*(5), 658–702. . https://doi.org/10.2165/00003495-198938050-00002

Berendsen, H. J. C., van der Spoel, D., & van Drunen, R. (1995). GROMACS: A message-passing parallel molecular dynamics implementation. *Computer Physics Communications*, *91*(1-3), 43–56. https://doi.org/10.1016/0010-4655(95)00042-E

Breckenridge, A., & Jacob, R. (2019). Overcoming the legal and regulatory barriers to drug repurposing. *Nature Reviews. Drug Discovery*, *18*(1), 1–2. https://doi.org/10.1038/nrd.2018.92

Cao, B., Wang, Y., Wen, D., Liu, W., Wang, J., Fan, G., Ruan, L., Song, B., Cai, Y., Wei, M., Li, X., Xia, J., Chen, N., Xiang, J., Yu, T., Bai, T., Xie, X., Zhang, L., Li, C. … Wang, C. (2020). A trial of lopinavir–ritonavir in adults hospitalized with severe Covid-19. The *New* England *Journal of Medicine*, *382*(19), 1787–1799. https://doi.org/10.1056/NEJMoa2001282

Cermelli, C., Cuoghi, A., Scuri, M., Bettua, C., Neglia, R. G., Ardizzoni, A., Blasi, E., Iannitti, T., & Palmieri, B. (2011). In vitro evaluation of antiviral and virucidal activity of a high molecular weight hyaluronic acid. *Virology Journal*, *8*(1), 141. https://doi.org/10.1186/1743-422X-8-141

Chandwani, A., & Shuter, J. (2008). Lopinavir/ritonavir in the treatment of HIV-1 infection: A review. *Therapeutics and Clinical Risk Management*, *4*(5), 1023–1033. https://doi.org/10.2147/TCRM.S3285

(2020). COVID-19 ring-based prevention trial with lopinavir/ritonavir – Full text view – ClinicalTrials.gov. Retrieved April 29, 2020, from https://clinicaltrials.gov/ct2/show/NCT04321174

David, C. C., & Jacobs, D. J. (2014). Principal component analysis: A method for determining the essential dynamics of proteins BT. In D. R. Livesay (Ed.), *Protein dynamics: Methods and protocols* (pp. 193–226). Totowa, NJ: Humana Press. https://doi.org/10.1007/978-1-62703-658-0_11.

Davidson, R. N., den Boer, M., & Ritmeijer, K. (2009). Paromomycin. *Transactions of the Royal Society of Tropical Medicine and Hygiene*, *103*(7), 653–660. https://doi.org/10.1016/j.trstmh.2008.09.008

DiNicolantonio, J. J., Bhutani, J., & O'Keefe, J. H. (2015). Acarbose: Safe and effective for lowering postprandial hyperglycaemia and improving cardiovascular outcomes. *Open Heart*, *2*(1), e000327. https://doi.org/10.1136/openhrt-2015-000327

Ennifar, E., Paillart, J.-C., Bodlenner, A., Walter, P., Weibel, J.-M., Aubertin, A.-M., Pale, P., Dumas, P., & Marquet, R. (2006). Targeting the dimerization initiation site of HIV-1 RNA with aminoglycosides: From crystal to cell. *Nucleic Acids Research*, *34*(8), 2328–2339. https://doi.org/10.1093/nar/gkl317

Fraser, J. R. E., Laurent, T. C., & Laurent, U. B. G. (1997). Hyaluronan: Its nature, distribution, functions and turnover. *Journal of Internal Medicine*, *242*(1), 27–33. https://doi.org/10.1046/j.1365-2796.1997.00170.x

Friesner, R. A., Murphy, R. B., Repasky, M. P., Frye, L. L., Greenwood, J. R., Halgren, T. A., Sanschagrin, P. C., Mainz, D. T., Friesner, R. A., Murphy, R. B., Repasky, M. P., Frye, L. L., Greenwood, J. R., Halgren, T. A., Sanschagrin, P. C., & Mainz, D. T. (2006). Extra precision glide: Docking and scoring incorporating a model of hydrophobic enclosure for

protein-ligand complexes. *Journal of Medicinal Chemistry*, *49*(21), 6177–6196. https://doi.org/10.1021/jm051256o

Giri, R., Bhardwaj, T., Shegane, M., Gehi, B. R., Kumar, P., Gadhave, K., Oldfield, C. J., & Uversky, V. N. (2020). When darkness becomes a ray of light in the dark times: Understanding the COVID-19 via the comparative analysis of the dark proteomes of SARS-CoV-2, human SARS and bat SARS-like coronaviruses. BioRxiv, 2020.03.13.990598. https://doi.org/10.1101/2020.03.13.990598.

Halgren, T. A. (2009). Identifying and characterizing binding sites and assessing druggability. *Journal of Chemical Information and Modeling*, *49*(2), 377–389. https://doi.org/10.1021/ci800324m

Halgren, T. A., Murphy, R. B., Friesner, R. A., Beard, H. S., Frye, L. L., Pollard, W. T., & Banks, J. L. (2004). Glide: A new approach for rapid, accurate docking and scoring. 2. Enrichment factors in database screening. *Journal of Medicinal Chemistry*, *47*(7), 1750–1759. https://doi.org/10.1021/jm030644s

Hess, B., Bekker, H., Berendsen, H. J. C., & Fraaije, J. G. E. M. (1997). LINCS: A linear constraint solver for molecular simulations. *Journal of Computational Chemistry*, *18*(12), 1463–1472. https://doi.org/10.1002/(SICI)1096-987X(199709)18:12<1463::AID-JCC4>3.0.CO;2-H

Hofland, L. J., & Lamberts, S. W. J. (1996). Somatostatin receptors and disease: Role of receptor subtypes. Baillière's *Clinical Endocrinology and Metabolism*, *10*(1), 163–176. https://doi.org/10.1016/S0950-351X(96)80362-4

Humphrey, W., Dalke, A., & Schulten, K. (1996). VMD: Visual molecular dynamics. *Journal of Molecular Graphics*, *14*(1), 33–38. https://doi.org/10.1016/0263-7855(96)00018-5

Jacobson, M. P., Pincus, D. L., Rapp, C. S., Day, T. J. F., Honig, B., Shaw, D. E., & Friesner, R. A. (2004). A hierarchical approach to all-atom protein loop prediction. *Proteins: Structure, Function, and Bioinformatics*, *55*(2), 351–367. https://doi.org/10.1002/prot.10613

Jin, Z., Du, X., Xu, Y., Deng, Y., Liu, M., Zhao, Y., Zhang, B., Li, X., Zhang, L., Peng, C., Duan, Y., Yu, J., Wang, L., Yang, K., Liu, F., Jiang, R., Yang, X., You, T., Liu, X. … Yang, H. (2020). Structure of Mpro from COVID-19 virus and discovery of its inhibitors. Nature, *582*(7811), 289–293. https://doi.org/10.1038/s41586-020-2223-y

Khalili, J. S., Zhu, H., Mak, N. S. A., Yan, Y., & Zhu, Y. (2020). Novel coronavirus treatment with ribavirin: Groundwork for an evaluation concerning COVID-19. *Journal of Medical Virology*, *92*(7), 740–746. https://doi.org/10.1002/jmv.25798

Khan, R. J., Jha, R. K., Amera, G. M., Jain, M., Singh, E., Pathak, A., Singh, R. P., Muthukumaran, J., & Singh, A. K. (2020). Targeting SARS-CoV-2: A systematic drug repurposing approach to identify promising inhibitors against 3C-like proteinase and 2′-O-ribose methyltransferase. *Journal of Biomolecular Structure and Dynamics*, 1–14. https://doi.org/10.1080/07391102.2020.1753577.

Krilov, L. R. (2001). Respiratory syncytial virus: Update on infection, treatment, and prevention. *Current Infectious Disease Reports*, *3*(3), 242–246. https://doi.org/10.1007/s11908-001-0026-3

Kumar, A., Liang, B., Aarthy, M., Singh, S. K., Garg, N., Mysorekar, I. U., & Giri, R. (2018). Hydroxychloroquine inhibits Zika virus NS2B-NS3 protease. *ACS Omega.*, *3*(12), 18132–18141. https://doi.org/10.1021/acsomega.8b01002

Kumar, D., Aarthy, M., Kumar, P., Singh, S. K., Uversky, V. N., & Giri, R. (2020). Targeting the NTPase site of Zika virus NS3 helicase for inhibitor discovery. *Journal of Biomolecular Structure & Dynamics*, *38*(16), 4811–4827. https://doi.org/10.1080/07391102.2019.1689851

Kumar, D., Sharma, N., Aarthy, M., Singh, S. K., & Giri, R. (2020). Mechanistic insights into Zika virus NS3 helicase inhibition by epigallocatechin-3-gallate. *ACS Omega*, *5*(19), 11217–11226. https://doi.org/10.1021/acsomega.0c01353

Kumar, P., Kumar, D., & Giri, R. (2019). Targeting the nsp2 cysteine protease of chikungunya virus using FDA approved library and selected cysteine protease inhibitors. *Pathogens*, *8*(3), 128. https://doi.org/10.3390/pathogens8030128

Kumar, P., Saumya, K. U., & Giri, R. (2020). Identification of peptidomimetic compounds as potential inhibitors against MurA enzyme of Mycobacterium tuberculosis. *Journal of Biomolecular Structure & Dynamics*, *38*(17), 4917–4997. https://doi.org/10.1080/07391102.2019.1696231

Kumar, Y., Singh, H., & Patel, C. N. (2020). In silico prediction of potential inhibitors for the Main protease of SARS-CoV-2 using molecular docking and dynamics simulation based drug-repurposing. *Journal of Infection and Public Health*, *13*(9), 1210–1223. https://doi.org/10.1016/j.jiph.2020.06.016

Li, J., Lim, S. P., Beer, D., Patel, V., Wen, D., Tumanut, C., Tully, D. C., Williams, J. A., Jiricek, J., Priestle, J. P., Harris, J. L., & Vasudevan, S. G. (2005). Functional profiling of recombinant NS3 proteases from all four serotypes of dengue virus using tetrapeptide and octapeptide substrate libraries. *The Journal of Biological Chemistry*, *280*(31), 28766–28774. https://doi.org/10.1074/jbc.M500588200

Loustaud-Ratti, V., Debette-Gratien, M., Jacques, J., Alain, S., Marquet, P., Sautereau, D., Rousseau, A., & Carrier, P. (2016). Ribavirin: Past, present and future. *World Journal of Hepatology*, *8*(2), 123–130. https://doi.org/10.4254/wjh.v8.i2.123

Madhavi Sastry, G., Adzhigirey, M., Day, T., Annabhimoju, R., & Sherman, W. (2013). Protein and ligand preparation: Parameters, protocols, and influence on virtual screening enrichments. *Journal of Computer-Aided Molecular Design*, *27*(3), 221–234. https://doi.org/10.1007/s10822-013-9644-8

McKeage, K., Cheer, S., & Wagstaff, A. J. (2003). Octreotide long-acting release (LAR): A review of its use in the management of acromegaly. Drugs, *63*(22), 2473–2499. https://doi.org/10.2165/00003495-200363220-00014

McMullan, B. J., & Mostaghim, M. (2015). Prescribing azithromycin. *Australian Prescriber*, *38*(3), 87–90. https://doi.org/10.18773/austprescr.2015.030

Muralidharan, N., Sakthivel, R., Velmurugan, D., & Gromiha, M. M. (2020). Computational studies of drug repurposing and synergism of lopinavir, oseltamivir and ritonavir binding with SARS-CoV-2 protease against COVID-19. *Journal of Biomolecular Structure and Dynamics*, 1–6. https://doi.org/10.1080/07391102.2020.1752802.

Peters, D. H., Friedel, H. A., & McTavish, D. (1992). Azithromycin. Drugs, *44*(5), 750–799. https://doi.org/10.2165/00003495-199244050-00007

Pushpakom, S., Iorio, F., Eyers, P. A., Escott, K. J., Hopper, S., Wells, A., Doig, A., Guilliams, T., Latimer, J., McNamee, C., Norris, A., Sanseau, P., Cavalla, D., & Pirmohamed, M. (2019). Drug repurposing: Progress, challenges and recommendations. *Nature Reviews. Drug Discovery*, *18*(1), 41–58. https://doi.org/10.1038/nrd.2018.168

Ramirez, M. S., & Tolmasky, M. E. (2017). Amikacin: Uses, resistance, and prospects for inhibition. Molecules, *22*(12), 2267. https://doi.org/10.3390/molecules22122267

Reddy, K. R., Nelson, D. R., & Zeuzem, S. (2009). Ribavirin: Current role in the optimal clinical management of chronic hepatitis C. *Journal of Hepatology*, *50*(2), 402–411. https://doi.org/10.1016/j.jhep.2008.11.006

(2020). Safety and efficacy of hydroxychloroquine associated with azithromycin in SARS-CoV2 virus (Coalition Covid-19 Brasil II) – Full text view – ClinicalTrials.gov. Retrieved April 29, 2020, from https://clinicaltrials.gov/ct2/show/NCT04321278

Sang, P., Tian, S.-H., Meng, Z.-H., & Yang, L.-Q. (2020). Anti-HIV drug repurposing against SARS-CoV-2. *RSC Advances*, *10*(27), 15775–15783. https://doi.org/10.1039/D0RA01899F

Shalev-Benami, M., Zhang, Y., Rozenberg, H., Nobe, Y., Taoka, M., Matzov, D., Zimmerman, E., Bashan, A., Isobe, T., Jaffe, C. L., Yonath, A., & Skiniotis, G. (2017). Atomic resolution snapshot of Leishmania ribosome inhibition by the aminoglycoside paromomycin. *Nature Communications*, *8*(1), 1589. https://doi.org/10.1038/s41467-017-01664-4

Sharma, N., Kumar, P., & Giri, R. (2020). Polysaccharides like pentagalloylglucose, parishin A and stevioside inhibits the viral entry by binding the Zika virus envelope protein. *Journal of Biomolecular Structure and Dynamics*, 1–13. https://doi.org/10.1080/07391102.2020.1797538

Sharma, N., Murali, A., Singh, S. K., & Giri, R. (2017). Epigallocatechin gallate, an active green tea compound inhibits the Zika virus entry into host cells via binding the envelope protein. *International Journal of Biological Macromolecules*, *104*(Pt A), 1046–1054. https://doi.org/10.1016/j.ijbiomac.2017.06.105

Shirley, M. (2019). Amikacin liposome inhalation suspension: A review in Mycobacterium avium complex lung disease. Drugs, *79*(5), 555–562. https://doi.org/10.1007/s40265-019-01095-z

Tamma, P. D., Cosgrove, S. E., & Maragakis, L. L. (2012). Combination therapy for treatment of infections with gram-negative bacteria. *Clinical Microbiology Reviews*, *25*(3), 450–470. https://doi.org/10.1128/CMR.05041-11

U.S. National Library of Medicine. (2020). Evaluation of the efficacy of the hydroxychloroquine-azithromycin combination in the in the prevention of COVID-19 related SDRA – Full Text View – ClinicalTrials.gov. Retrieved April 29, 2020, from https://clinicaltrials.gov/ct2/show/NCT04347512

Victorovich, K. V., Rajanish, G., Aleksandrovna, K. T., Krishna, K. S., Nicolaevich, S. A., & Vitoldovich, P. V. (2020). Translation-associated mutational U-pressure in the first ORF of SARS-CoV-2 and other coronaviruses. BioRxiv, 2020.05.05.078238. https://doi.org/10.1101/2020.05.05.078238.

Widjaja, L. K., Bora, M., Chan, P. N. P. H., Lipik, V., Wong, T. T. L., & Venkatraman, S. S. (2014). Hyaluronic acid-based nanocomposite hydrogels for ocular drug delivery applications. *Journal of Biomedical Materials Research Part A*, *102*(9), 3056–3065. https://doi.org/10.1002/jbm.a.34976

Wishart, D. S., Feunang, Y. D., Guo, A. C., Lo, E. J., Marcu, A., Grant, J. R., Sajed, T., Johnson, D., Li, C., Sayeeda, Z., Assempour, N., Iynkkaran, I., Liu, Y., Maciejewski, A., Gale, N., Wilson, A., Chin, L., Cummings, R., Le, D., … Wilson, M. (2018). DrugBank 5.0: A major update to the DrugBank database for 2018. *Nucleic Acids Research*, *46*(D1), D1074–D1082. https://doi.org/10.1093/nar/gkx1037

Wu, C., Liu, Y., Yang, Y., Zhang, P., Zhong, W., Wang, Y., Wang, Q., Xu, Y., Li, M., Li, X., Zheng, M., Chen, L., & Li, H. (2020). Analysis of therapeutic targets for SARS-CoV-2 and discovery of potential drugs by computational methods. *Acta Pharmaceutica Sinica. B*, *10*(5), 766–788. https://doi.org/10.1016/j.apsb.2020.02.008

Yadav, R., Selvaraj, C., Aarthy, M., Kumar, P., Kumar, A., Singh, S. K., & Giri, R. (2020). Investigating into the molecular interactions of flavonoids targeting NS2B-NS3 protease from Zika virus through in-silico approaches. *Journal of Biomolecular Structure and Dynamics*, 1–13. https://doi.org/10.1080/07391102.2019.1709546.

Zhang, L., Lin, D., Sun, X., Curth, U., Drosten, C., Sauerhering, L., Becker, S., Rox, K., & Hilgenfeld, R. (2020). Crystal structure of SARS-CoV-2 main protease provides a basis for design of improved α-ketoamide inhibitors. Science, *368*(6489), 409–412. https://doi.org/10.1126/science.abb3405